Search for B^{0} decays to invisible final states at Belle

C.-L. Hsu *et al.* (Belle Collaboration)

Phys. Rev. D **86**, 032002 — Published 1 August 2012

DOI: 10.1103/PhysRevD.86.032002

Search for B^0 Decays to Invisible Final States at Belle

C.-L. Hsu,[31] P. Chang,[31] I. Adachi,[9] H. Aihara,[48] K. Arinstein,[2] D. M. Asner,[37] V. Aulchenko,[2] T. Aushev,[15] A. M. Bakich,[43] B. Bhuyan,[10] M. Bischofberger,[29] A. Bondar,[2] G. Bonvicini,[53] A. Bozek,[32] M. Bračko,[24,16] T. E. Browder,[8] M.-C. Chang,[5] Y. Chao,[31] V. Chekelian,[25] A. Chen,[30] P. Chen,[31] B. G. Cheon,[7] K. Chilikin,[15] I.-S. Cho,[55] K. Cho,[19] Y. Choi,[42] J. Dalseno,[25,45] J. Dingfelder,[1] Z. Doležal,[3] Z. Drásal,[3] D. Dutta,[10] S. Eidelman,[2] D. Epifanov,[2] S. Esen,[4] H. Farhat,[53] J. E. Fast,[37] V. Gaur,[44] N. Gabyshev,[2] R. Gillard,[53] Y. M. Goh,[7] J. Haba,[9] T. Hara,[9] K. Hayasaka,[28] H. Hayashii,[29] Y. Horii,[28] Y. Hoshi,[46] W.-S. Hou,[31] Y. B. Hsiung,[31] H. J. Hyun,[21] T. Iijima,[28,27] K. Inami,[27] A. Ishikawa,[47] R. Itoh,[9] M. Iwabuchi,[55] Y. Iwasaki,[9] T. Iwashita,[29] T. Julius,[26] J. H. Kang,[55] T. Kawasaki,[34] H. Kichimi,[9] C. Kiesling,[25] H. J. Kim,[21] H. O. Kim,[21] J. B. Kim,[20] J. H. Kim,[19] K. T. Kim,[20] Y. J. Kim,[19] B. R. Ko,[20] P. Kodyš,[3] S. Korpar,[24,16] P. Krokovny,[2] T. Kuhr,[18] A. Kuzmin,[2] P. Kvasnička,[3] Y.-J. Kwon,[55] S.-H. Lee,[20] J. Li,[41] Y. Li,[52] J. Libby,[11] Y. Liu,[4] Z. Q. Liu,[12] D. Liventsev,[15] R. Louvot,[22] K. Miyabayashi,[29] H. Miyata,[34] Y. Miyazaki,[27] G. B. Mohanty,[44] A. Moll,[25,45] N. Muramatsu,[39] E. Nakano,[36] M. Nakao,[9] Z. Natkaniec,[32] C. Ng,[48] S. Nishida,[9] O. Nitoh,[51] T. Ohshima,[27] S. Okuno,[17] S. L. Olsen,[41,8] G. Pakhlova,[15] C. W. Park,[42] H. Park,[21] H. K. Park,[21] T. K. Pedlar,[23] R. Pestotnik,[16] M. Petrič,[16] L. E. Piilonen,[52] M. Ritter,[25] M. Röhrken,[18] S. Ryu,[41] H. Sahoo,[8] Y. Sakai,[9] S. Sandilya,[44] T. Sanuki,[47] O. Schneider,[22] C. Schwanda,[13] A. J. Schwartz,[4] K. Senyo,[54] M. E. Sevior,[26] M. Shapkin,[14] C. P. Shen,[27] T.-A. Shibata,[49] J.-G. Shiu,[31] B. Shwartz,[2] A. Sibidanov,[43] F. Simon,[25,45] J. B. Singh,[38] P. Smerkol,[16] Y.-S. Sohn,[55] E. Solovieva,[15] S. Stanič,[35] M. Starič,[16] M. Sumihama,[6] T. Sumiyoshi,[50] G. Tatishvili,[37] Y. Teramoto,[36] K. Trabelsi,[9] M. Uchida,[49] T. Uglov,[15] Y. Unno,[7] S. Uno,[9] P. Urquijo,[1] Y. Usov,[2] S. E. Vahsen,[8] P. Vanhoefer,[25] G. Varner,[8] V. Vorobyev,[2] P. Wang,[12] M. Watanabe,[34] Y. Watanabe,[17] K. M. Williams,[52] E. Won,[20] H. Yamamoto,[47] Y. Yamashita,[33] Z. P. Zhang,[40] V. Zhilich,[2] and V. Zhulanov[2]

(The Belle Collaboration)

[1]*University of Bonn, Bonn*
[2]*Budker Institute of Nuclear Physics SB RAS and Novosibirsk State University, Novosibirsk 630090*
[3]*Faculty of Mathematics and Physics, Charles University, Prague*
[4]*University of Cincinnati, Cincinnati, Ohio 45221*
[5]*Department of Physics, Fu Jen Catholic University, Taipei*
[6]*Gifu University, Gifu*
[7]*Hanyang University, Seoul*
[8]*University of Hawaii, Honolulu, Hawaii 96822*
[9]*High Energy Accelerator Research Organization (KEK), Tsukuba*
[10]*Indian Institute of Technology Guwahati, Guwahati*
[11]*Indian Institute of Technology Madras, Madras*
[12]*Institute of High Energy Physics, Chinese Academy of Sciences, Beijing*
[13]*Institute of High Energy Physics, Vienna*
[14]*Institute of High Energy Physics, Protvino*
[15]*Institute for Theoretical and Experimental Physics, Moscow*
[16]*J. Stefan Institute, Ljubljana*
[17]*Kanagawa University, Yokohama*
[18]*Institut für Experimentelle Kernphysik, Karlsruher Institut für Technologie, Karlsruhe*
[19]*Korea Institute of Science and Technology Information, Daejeon*
[20]*Korea University, Seoul*
[21]*Kyungpook National University, Taegu*
[22]*École Polytechnique Fédérale de Lausanne (EPFL), Lausanne*
[23]*Luther College, Decorah, Iowa 52101*
[24]*University of Maribor, Maribor*
[25]*Max-Planck-Institut für Physik, München*
[26]*University of Melbourne, School of Physics, Victoria 3010*
[27]*Graduate School of Science, Nagoya University, Nagoya*
[28]*Kobayashi-Maskawa Institute, Nagoya University, Nagoya*
[29]*Nara Women's University, Nara*
[30]*National Central University, Chung-li*
[31]*Department of Physics, National Taiwan University, Taipei*
[32]*H. Niewodniczanski Institute of Nuclear Physics, Krakow*
[33]*Nippon Dental University, Niigata*

[34]*Niigata University, Niigata*
[35]*University of Nova Gorica, Nova Gorica*
[36]*Osaka City University, Osaka*
[37]*Pacific Northwest National Laboratory, Richland, Washington 99352*
[38]*Panjab University, Chandigarh*
[39]*Research Center for Electron Photon Science, Tohoku University, Sendai*
[40]*University of Science and Technology of China, Hefei*
[41]*Seoul National University, Seoul*
[42]*Sungkyunkwan University, Suwon*
[43]*School of Physics, University of Sydney, NSW 2006*
[44]*Tata Institute of Fundamental Research, Mumbai*
[45]*Excellence Cluster Universe, Technische Universität München, Garching*
[46]*Tohoku Gakuin University, Tagajo*
[47]*Tohoku University, Sendai*
[48]*Department of Physics, University of Tokyo, Tokyo*
[49]*Tokyo Institute of Technology, Tokyo*
[50]*Tokyo Metropolitan University, Tokyo*
[51]*Tokyo University of Agriculture and Technology, Tokyo*
[52]*CNP, Virginia Polytechnic Institute and State University, Blacksburg, Virginia 24061*
[53]*Wayne State University, Detroit, Michigan 48202*
[54]*Yamagata University, Yamagata*
[55]*Yonsei University, Seoul*

We report a search for B^0 decays into invisible final states using a data sample of 657×10^6 $B\overline{B}$ pairs collected at the $\Upsilon(4S)$ resonance with the Belle detector at the KEKB e^+e^- collider. The signal is identified by fully reconstructing a hadronic decay of the accompanying B meson and requiring no other particles in the event. No significant signal is observed, and we obtain an upper limit of 1.3×10^{-4} at the 90% confidence level for the branching fraction of invisible B^0 decay.

PACS numbers: 13.20.He,12.15.Ji,12.60.Jv

In the Standard Model (SM), the decay $B^0 \to \nu\overline{\nu}$ proceeds through the three annihilation diagrams shown in Fig. 1(a). This decay is highly helicity-suppressed with an expected branching fraction at the 10^{-20} level [1]. Because neutrinos participate only in weak interactions, the experimental signature is missing energy and momentum corresponding to the presence of a B^0 meson in the event. New particles hypothesized by physics beyond the SM, such as R-parity violating supersymmetry, can be involved in these B decays, resulting in a final state with only weakly interacting particles and providing the same signature as in $B^0 \to \nu\overline{\nu}$. For instance, Ref. [2] discusses the B decay into a neutrino and a neutralino ($\tilde{\chi}_1^0$), shown in Fig. 1(b); the branching fraction could be as high as $10^{-6} - 10^{-7}$. Therefore, signals of invisible B decays in current B factory data would indicate new physics. So far no such signals were observed. The first experimental result was provided by the BaBar collaboration, with $\mathcal{B}(B \to \text{invisible}) < 2.2 \times 10^{-4}$ at the 90% confidence level [3] with a semileptonic tagging method; recently, the upper limit was pushed to 2.4×10^{-5} with more data and improved tagging efficiency by BaBar [4].

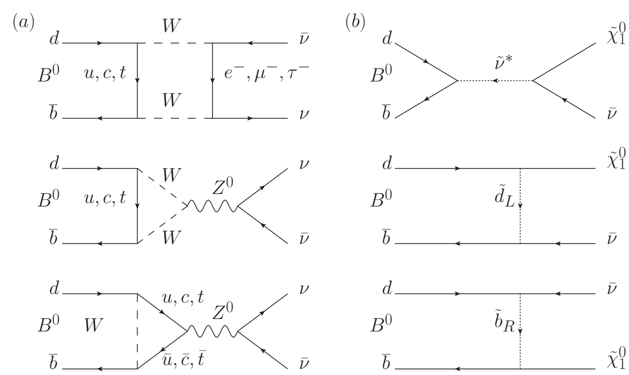

FIG. 1: Feynman diagrams for the SM process via $B^0 \to \nu\overline{\nu}$ (a) and for new physics via $B^0 \to \tilde{\chi}_1^0\overline{\nu}$ (b)[2].

In this paper we report the result of a search for B decays to an invisible final state based on the data collected with the Belle detector at the KEKB asymmetric-energy (3.5 on 8 GeV) e^+e^- collider [5]. The data sample consists of 657×10^6 $B\overline{B}$ pairs accumulated at the $\Upsilon(4S)$ resonance, corresponding to an integrated luminosity of 606 fb^{-1}, and an additional 68 fb^{-1} of off-resonance data recorded at a center-of-mass (CM) energy about 60 MeV below the $\Upsilon(4S)$ resonance. The Belle detector consists of a 4-layer silicon vertex detector (SVD), a 50-layer central drift chamber (CDC), time-of-flight scintillation counters (TOF), an array of aerogel threshold Cherenkov counters (ACC), and a CsI(Tl) electromagnetic calorimeter(ECL) located inside a superconducting solenoid coil that provides a 1.5 T magnetic field. Outside the coil, the K_L^0 and muon detector (KLM), composed of resistive plate counters, detects K_L^0 mesons and identifies muons. The detector is described in detail elsewhere [6]. A GEANT3-based [7] Monte Carlo (MC) simulation of the Belle detector is used to optimize the event selection and to estimate the signal efficiency.

Since the $\Upsilon(4S)$ decays to $B\overline{B}$ pairs, invisible B decay candidates are identified by fully reconstructing a B meson ($B_{\rm tag}$) following the procedure of Ref. [8] in hadronic modes, and then examining whether there are any other particles in the event. The neutral $B_{\rm tag}$ candidates are reconstructed through $B^0 \to D^{(*)-}h^+$ decays, where h^+ denotes π^+, ρ^+, a_1^+, or $D_s^{(*)+}$ [9]. Candidate $D^*_{(s)}$ mesons are identified through the channels $D_s^{*+} \to D_s^+\gamma$ and $D^{*-} \to \overline{D}^0\pi^-$. Candidate $D_{(s)}$ mesons are reconstructed using the following final states: $K^-\pi^+\pi^+$, $K^-\pi^+\pi^+\pi^0$, $K^+K^-\pi^+$, $K_S^0\pi^+, K_S^0\pi^+\pi^0$, and $K_S^0\pi^+\pi^+\pi^-$ for D^+; $K^-\pi^+$, $K_S^0\pi^0, K^+K^-$, $K^-\pi^+\pi^0$, $K_S^0\pi^+\pi^-$, $K^-\pi^+\pi^+\pi^-$, and $K_S^0\pi^+\pi^-\pi^0$ for D^0; and $K_S^0K^+, K^+\pi^-\pi^+$, and $K^+K^-\pi^+$ for D_s^+.

Charged kaons and pions are identified using specific ionization from the CDC, time-of-flight information from the TOF, and Cherenkov light yield in the ACC. This information is combined to form a K-π likelihood ratio $\mathcal{R}_{K/\pi} = \mathcal{L}_K/(\mathcal{L}_K + \mathcal{L}_\pi)$, where $\mathcal{L}_K$ ($\mathcal{L}_\pi$) is the likelihood that the track is a kaon (pion). Tracks with $\mathcal{R}_{K/\pi} > 0.6$ are regarded as kaons and $\mathcal{R}_{K/\pi} < 0.4$ as pions. The typical selection efficiency for a 1.0 GeV/c kaon (pion) is 83% (90%) while the misidentification probability for 1.0 GeV/c kaons (pions) as pions (kaons) is around 6% (12%). Neutral $K_S^0 \to \pi^+\pi^-$ candidates are identified by pairing two opposite-sign charged tracks, both treated as pions, then requiring that this pair have an invariant mass near the nominal K_S^0 mass with a vertex displaced from the e^+e^- interaction point. Candidate K_L^0's are selected from KLM hit patterns that are not associated with any charged track [10]. Neutral pions are identified using the $\pi^0 \to \gamma\gamma$ decay and requiring each photon to have a minimum energy of 50 MeV and $\gamma\gamma$ mass between 0.115 GeV/c^2 and 0.156 GeV/c^2. The ρ^+ and a_1^+ meson candidates are reconstructed using the $\rho^+ \to \pi^+\pi^0$ and $a_1^+ \to \pi^+\pi^-\pi^+$ channels.

The selection of $B_{\rm tag}$ candidates is based on two kinematic variables: the beam-energy constrained mass $M_{\rm bc} \equiv \sqrt{E^2_{\rm beam} - p^2_B}$ and the energy difference $\Delta E \equiv E_B - E_{\rm beam}$, where E_B and p_B are the reconstructed energy and momentum of the $B_{\rm tag}$ candidate in the e^+e^- CM frame, and $E_{\rm beam}$ is the beam energy in this frame. The $B_{\rm tag}$ candidates are required to have $M_{\rm bc} > 5.22\,{\rm GeV}/c^2$ and $|\Delta E| < 0.3\,{\rm GeV}$. Within this region, we define the signal region: 5.27 GeV/c^2 $< M_{\rm bc} <$ 5.29 GeV/c^2 and -0.08 GeV $< \Delta E <$ 0.06 GeV. Figure 2 shows the $M_{\rm bc}$ and ΔE distributions of the $B_{\rm tag}$ candidates in data. If there are multiple $B_{\rm tag}$ candidates in an event, the candidate with the smallest χ^2 is retained, where χ^2 is computed using ΔE, the D meson mass, the mass difference between the D^* and D (for candidates with a D^* in the final state), weighted using their expected resolutions. We reconstruct 9.5×10^5 neutral $B_{\rm tag}$ candidates in total. After identifying the $B_{\rm tag}$ candidate, we require no additional charged tracks nor π^0 or K_L^0 candidates in the rest of the event.

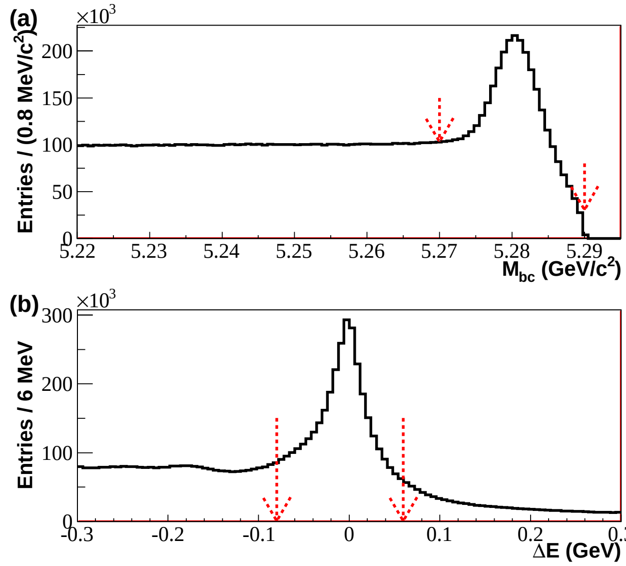

FIG. 2: The $M_{\rm bc}$ (a) and ΔE (b) distributions for the $B_{\rm tag}$ candidates. Candidates having $M_{\rm bc}$ and ΔE within the signal regions between the two arrows are used to search for B decays to invisible final states.

The dominant backgrounds are from $e^+e^- \to q\overline{q}$ ($q = u, d, s, c$) continuum events and $B\overline{B}$ decays with a $b \to c$ transition (generic B background). Two variables are used to distinguish the signal and continuum events: $\cos\theta_B$, defined as the cosine of the angle between the $B_{\rm tag}$ flight direction and the beam axis in the CM frame, and $\cos\theta_T$, the cosine of the angle of the $B_{\rm tag}$ thrust axis with respect to the beam axis in the CM frame. Clear differences in the distribution of each variable between signal and continuum background are shown in Fig. 3, using the MC simulation. We define the fit region as $-0.9 < \cos\theta_B < 0.9$ and $-0.6 < \cos\theta_T < 0.6$. The variable $\cos\theta_B$ is used in the fit to extract the signal yield. Other backgrounds, such as rare B decays via $b \to q$ ($q = u, d, s$) processes and $e^+e^- \to \tau^+\tau^-$ transitions, are also considered in the signal extraction and studied using large MC samples. The $\tau^+\tau^-$ background is small and has an event topology similar to the continuum; therefore, the continuum and $\tau^+\tau^-$ backgrounds are combined and called the non-B background.

The most powerful variable to identify B decays into the invisible final state is the residual energy in the ECL, denoted $E_{\rm ECL}$, which is the sum of the energies of ECL clusters that are not associated with the $B_{\rm tag}$ daughters. To further suppress the background, minimum energy thresholds are required for clusters located in various ECL regions: 50 MeV for the barrel ($32.2^\circ < \theta < 128.7^\circ$), 100 MeV for the forward endcap ($\theta < 32.2^\circ$), and 150 MeV for the backward endcap ($\theta > 128.7^\circ$).

The signal yield for invisible B decays is extracted from an extended unbinned maximum likelihood fit to

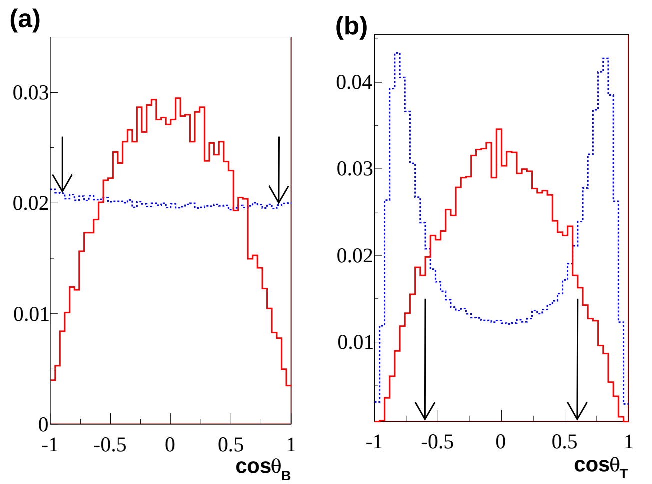

FIG. 3: Normalized distributions of (a) $\cos\theta_B$ and (b) $\cos\theta_T$ for the signal and continuum backgrounds. The solid histogram is the signal and the dashed histogram is the continuum background.

the $E_{\rm ECL}$ and $\cos\theta_B$ distributions. The likelihood is

$$\mathcal{L} = \frac{e^{-\sum_j n_j}}{N!} \prod_{i=1}^{N} \left(\sum_j n_j \mathcal{P}_j^i(E_{\rm ECL}, \cos\theta_B) \right), \qquad (1)$$

where i is the event identifier; n_j is the yield for category j, which corresponds to either signal, generic B, rare B or non-B background; and $\mathcal{P}_j(E_{\rm ECL}, \cos\theta_B)$ is the product of the probability density functions (PDFs) $\mathcal{P}(E_{\rm ECL})$ and $\mathcal{P}(\cos\theta_B)$, since we have verified that $E_{\rm ECL}$ and $\cos\theta_B$ are uncorrelated for each component. For each category, the $E_{\rm ECL}$ PDF is modeled as a histogram function, while the $\cos\theta_B$ PDF is described by a 1$^{\rm st}$ or 2$^{\rm nd}$ order Legendre polynomial. The non-B $E_{\rm ECL}$ PDF is constructed from off-resonance data, while all other PDFs are obtained using MC simulations. The normalization of the rare B background category is estimated from the MC simulation and is fixed in the fit.

The $E_{\rm ECL}$ simulation is validated using doubly-tagged events in which the $B_{\rm tag}$ is fully reconstructed as described above and the other B is identified as $B^0 \to D^{(*)-}\ell^+\nu$ ($\ell = e, \mu$). Candidate D^{*-} mesons are reconstructed via $D^{*-} \to \overline{D}^0\pi^-$, followed by $\overline{D}^0 \to K^+\pi^-$, while D^- is identified as $D^- \to K_S^0\pi^-$ and $K^+\pi^-\pi^-$. The track and π^0selections are applied here. Background contributions in the doubly-tagged sample are found to be negligible; therefore, only loose selections on D and D^* masses and the mass squared of the undetected particles $m^2_{\rm miss} = |\mathbf{P}_{\rm beam} - \mathbf{P}_{B_{\rm tag}} - \mathbf{P}_{D^{(*)-}\ell^+}|^2$ (where $\mathbf{P}$ denotes the four-momentum of the e^+e^- system, $B_{\rm tag}$, or the $D^{(*)-}\ell^+$ system) are applied.

The observed $E_{\rm ECL}$ distributions for doubly-tagged events, shown in Fig. 4, are found to be in good agreement with MC simulations. The signal yields for control modes are obtained by fitting the $E_{\rm ECL}$ spectra while the efficiencies are estimated from MC samples. The measured branching fractions with their errors, listed in Table I, agree well with the PDG values [11]. The $B^0 \to D^{(*)-}\ell^+\nu$ decays are also used to study the systematic uncertainty arising due to the track, π^0, and K_L^0 rejections as well as to calibrate the signal efficiency. The aforementioned systematic uncertainties are estimated by comparing the efficiency before and after the application of those vetoes on data and MC. The data-MC efficiency ratios for track, π^0, and K_L^0 vetoes are 0.996 ± 0.012, 0.913 ± 0.020, and 1.096 ± 0.020, respectively. The central values are used to correct the MC efficiencies, while the statistical error is treated as a contribution to the systematic uncertainty. Since the central value of the track veto inefficiency is small, no scaling factor is applied on the veto efficiency. Instead, the sum of the inefficiency and the statistical error is quoted as a systematic uncertainty.

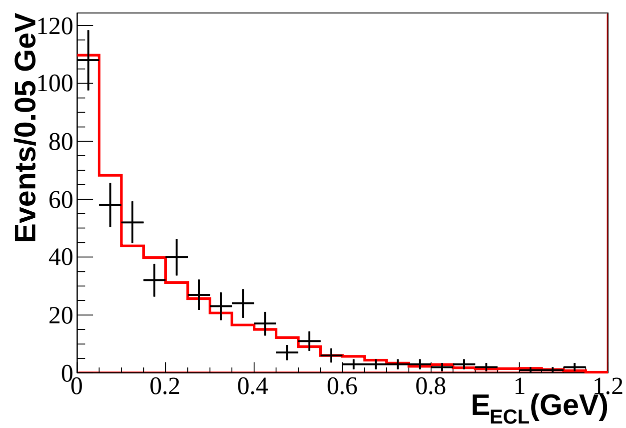

FIG. 4: $E_{\rm ECL}$ distribution for doubly-tagged events, in which one B is fully reconstructed and the other B is reconstructed as $B^0 \to D^{(*)-}\ell^+\nu$. Points with error bars are data and the solid histogram is a signal MC simulation.

TABLE I: Summary of the fit result for $B^0 \to D^{(*)-}\ell^+\nu$ samples (branching fractions in units of 10^{-3}). The second column and third column show the products of branching fractions, where the error on the second column is statistical only.

Mode	Measured result	PDG value[11]
$B^0 \to D^{*-}\mu^+\nu$	1.41 ± 0.20	1.34 ± 0.06
$B^0 \to D^{*-}e^+\nu$	1.62 ± 0.18	1.34 ± 0.06
$B^0 \to D^-(K\pi\pi)\mu^+\nu$	1.99 ± 0.21	1.98 ± 0.12
$B^0 \to D^-(K\pi\pi)e^+\nu$	1.93 ± 0.14	1.98 ± 0.12
$B^0 \to D^-(K_S^0\pi)\mu^+\nu$	0.19 ± 0.06	0.22 ± 0.02
$B^0 \to D^-(K_S^0\pi)e^+\nu$	0.21 ± 0.05	0.22 ± 0.02

Table II lists the signal and background yields for invisible B decays from the fit while Fig. 5 shows the $E_{\rm ECL}$

and $\cos\theta_B$ distributions superimposed with the fit result. No significant signal is observed. The signal efficiency, determined with MC simulations and later calibrated using the doubly-tagged $B^0 \to D^{(*)-}\ell^+\nu$ sample, is $(2.2 \pm 0.2) \times 10^{-4}$, where the error is dominated by the systematic uncertainty.

TABLE II: Summary of fit yields for the signal and background. The normalization of the rare B background contribution is fixed in the fit.

Component	Yield
Signal	$8.9^{+6.3}_{-5.5}$
Generic B background	$131.6^{+21.9}_{-22.8}$
Non-B background	$-23.2^{+21.6}_{-17.0}$
Rare B background	3.7
Observed events	121

The systematic uncertainty associated with the signal efficiency is dominated by the $B_{\rm tag}$ reconstruction efficiency. The uncertainty on $B_{\rm tag}$ reconstruction is estimated by comparing the yield difference between data and the corresponding MC sample, generated with a proper mixture of generic B and continuum events. The $B_{\rm tag}$ yields are extracted by fitting the $M_{\rm bc}$ distributions and an uncertainty of 8.3% is assigned. Systematic uncertainties arising from the requirement of no additional charged tracks nor π^0 and K_L^0 candidates are estimated to be 1.6%, 2.0% and 2.0%, respectively, using $B^0 \to D^{(*)-}\ell^+\nu$ decays in data. The uncertainty in the number of $B\overline{B}$ pairs is 1.4%.

TABLE III: Summary of systematic uncertainties arising from PDF modeling and components with fixed normalizations.

Source	Events
Signal PDF	negligible
Generic B PDF	$+1.6/-1.4$
Rare B PDF	± 0.1
Rare B fixed yield	$+0.2/-0.1$
Non-B PDF	$+1.9/-1.3$
Binning effect	$+1.7/-1.8$
Sum	$+3.0/-2.6$

The uncertainties in the signal yield extraction are summarized in Table III. The uncertainty due to fixing the normalization of the rare B component is obtained by varying the rare B yield by the estimated uncertainty (± 1.9 events). The corresponding variation in the signal yield, $^{+0.2}_{-0.1}$, is assigned as the systematic uncertainty. For each $E_{\rm ECL}$ PDF, we successively vary the content of each histogram bin by $\pm 1\sigma$ to obtain a new PDF. The variation in the signal yield using the new PDF is calculated by performing an unbinned likelihood fit; the quadratic sum of all the variations gives the systematic uncertainty

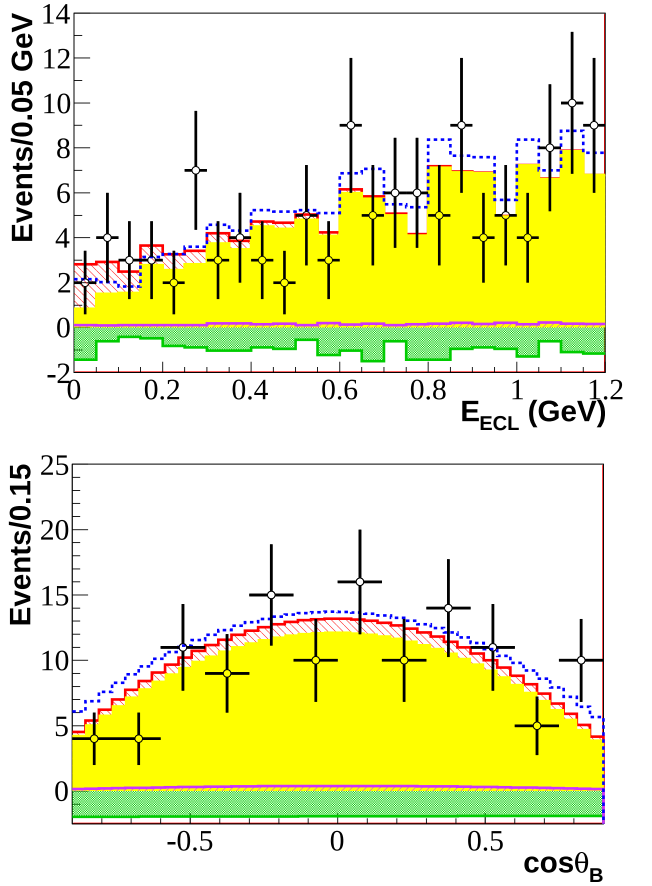

FIG. 5: The $E_{\rm ECL}$ (top) and $\cos\theta_B$ (bottom) distributions with fit results superimposed. Points with error bars are data. The red cross-hatched region is the signal component on the top of the total background shown in the yellow filled histogram. The blue dashed curve is the generic B contribution which is larger than the total because of the negative fit result for the non-B background shown in the green dotted histogram. The purple hatched area corresponds to the rare B contribution.

for the PDF. The systematic uncertainty arising from $\cos\theta_B$ PDFs is negligible. Moreover, the effect of bin size is also investigated by choosing different bin sizes to model the PDFs. Again, the variation in the signal yield is considered as a systematic uncertainty. The total systematic uncertainty is computed by summing all contributions listed in Table III in quadrature.

Since there is no significant signal observed, an upper limit at 90% confidence level (C.L.) is computed using the fit likelihood as a function of the branching fraction. The branching fraction is obtained from the signal yield from the fit, the signal selection efficiency and the number of $B\overline{B}$ pairs. The likelihood at each signal yield is obtained using Eq. 1 except that the signal yield is fixed in the fit. The systematic uncertainty of the measurement is taken into account by convolving the likelihood function with a Gaussian whose width equals the systematic uncertainty ($\Delta\mathcal{B}$),

$$\mathcal{L}_{\mathrm{smear}}(\mathcal{B}) = \int \mathcal{L}(\mathcal{B}') \frac{e^{-\frac{(\mathcal{B}-\mathcal{B}')^2}{2\Delta\mathcal{B}^2}}}{\sqrt{2\pi\Delta\mathcal{B}}} d\mathcal{B}'. \tag{2}$$

The upper limit on the branching fraction is estimated by integrating the likelihood function from zero to the bound that gives 90% of the total area. We obtain $\mathcal{B}(B \to \text{invisible}) < 1.3 \times 10^{-4}$ at the 90% C.L. The expected upper limit, estimated by applying the same method on the MC sample, is 1.1×10^{-4}.

In conclusion, we have performed a search for $B \to$ invisible decay with a fully reconstructed B_{tag} on a data sample of 657×10^6 $B\overline{B}$ pairs collected at the $\Upsilon(4S)$ resonance with the Belle detector. No significant signal is observed and we set an upper limit of 1.3×10^{-4} at the 90% confidence level for the branching fraction of invisible B decay. The limit obtained for $B^0 \to$ invisible decay is the most stringent constraint to date with a hadronic tagging method.

We thank the KEKB group for excellent operation of the accelerator; the KEK cryogenics group for efficient solenoid operations; and the KEK computer group, the NII, and PNNL/EMSL for valuable computing and SINET4 network support. We acknowledge support from MEXT, JSPS and Nagoya's TLPRC (Japan); ARC and DIISR (Australia); NSFC (China); MSMT (Czechia); DST (India); INFN (Italy); MEST, NRF, BRL program with grant no. KRF-2011-0020333, GSDC of KISTI, and WCU (Korea); MNiSW (Poland); MES and RFAAE (Russia); ARRS (Slovenia); SNSF (Switzerland); NSC and MOE (Taiwan); and DOE and NSF (USA).

[1] G. Buchalla and A. J. Buras, Nucl. Phys. B **400**, 225 (1993).
[2] A. Dedes, H. Dreiner, and P. Richardson, Phys. Rev. D **65**, 015001 (2001).
[3] B. Aubert *et al.* (BaBar Collaboration), Phys. Rev. Lett. **93**, 091802 (2004).
[4] J. P. Lees *et al.* (BaBar Collaboration), arXiv:1206.2543 [hep-ex].
[5] S. Kurokawa and E. Kikutani, Nucl. Instr. Meth. A **499**, 1 (2003), and other papers included in this volume.
[6] A. Abashian *et al.* (Belle Collaboration), Nucl. Instr. Meth. A **479**, 117 (2002).
[7] R. Brun *et al.*, GEANT 3.21, CERN Report No. DD/EE/84-1 (1987).
[8] K. Ikado *et al.* (Belle Collaboration), Phys. Rev. Lett. **97**, 251802 (2006).
[9] The inclusion of charge-conjugate modes is implied throughout this paper.
[10] K. Abe *et al.* (Belle Collaboration), Phys. Rev. Lett. **87**, 091802 (2001); Phys. Rev. D **66**, 071102 (2002).
[11] K. Nakamura *et al.* (Particle Data Group), J. Phys. G **37**, 075021 (2010) and 2011 partial update for the 2012 edition.